Angular dependence of magnetic dichroism and spin polarization in angle-resolved core-level photoemission

1999 J. Phys.: Condens. Matter 11 6475

(http://iopscience.iop.org/0953-8984/11/33/315)

J. Phys.: Condens. Matter **11** (1999) 6475–6486. Printed in the UK PII: S0953-8984(99)04332-5

Angular dependence of magnetic dichroism and spin polarization in angle-resolved core-level photoemission

A Chassé

Department of Physics, Martin-Luther-University Halle-Wittenberg, D-06099 Halle, Germany

E-mail: chasse@physik.uni-halle.de

Received 14 May 1999

Abstract. Photoelectron diffraction theory is applied to the investigation of the dependence of magnetic dichroism and spin polarization on the emission direction of photoelectrons in angle-resolved core-level photoemission. It is shown that photoelectron diffraction effects may cause significant modulations in the angular dependence of magnetic dichroism in angle-resolved core-level photoemission. Furthermore, it is pointed out that both magnetic dichroism and spin polarization should show the same angular dependence on the electron emission direction. Results of photoelectron diffraction theory are discussed in detail for p-type core-level photoemission in comparison with those of the single-atom approach. The applied theory gives a good explanation of the experimental data of Fe 3p and Co 2p photoelectrons excited in thin Fe and Co films, respectively.

1. Introduction

Magnetic dichroism in the angular distribution of photoelectrons (MDAD) from ferromagnets was observed first by Baumgarten *et al* [1] using circularly polarized light. Baumgarten observed that the recorded photoemission spectra of Fe 2p shows a pronounced dependence on the relative orientation of the photon spin and the direction of magnetization. This dichroism has been qualitatively explained by taking into account the spin–orbit splitting of the Fe 2p level in combination with exchange splitting of the corresponding sublevels [2, 3].

The first observation of MDAD prompted a flurry of both theoretical and experimental activities in the study of MDAD with circularly polarized light (MCDAD) [4–10]. It was soon realized that MDAD could also be observed using linearly polarized light (MLDAD) in an angle-resolved photoemission experiment with the proper geometry [11–13]. Even more remarkable was the first experimental observation of MDAD with unpolarized light [14]. Meanwhile this kind of dichroism, termed MUDAD, was studied for several itinerant ferromagnetic systems [15–18].

In principle, MDAD of photoelectrons using circularly polarized light can be measured by two distinct methods: fixing the magnetization and reversing the photon helicity, or fixing the photon helicity and reversing the magnetization. If linearly polarized or unpolarized light is used, the MDAD can only be observed by reversing the magnetization (figure 1). A first systematic overview and classification of the rather wide variety of magnetic dichroism effects in photoemission has been provided recently by Venus *et al* [5].

Until now, most theoretical work on MDAD has completely neglected the influence of photoelectron diffraction (PD) effects [2, 3, 19–21]. However, in general, this is not a valid

0953-8984/99/336475+12$30.00

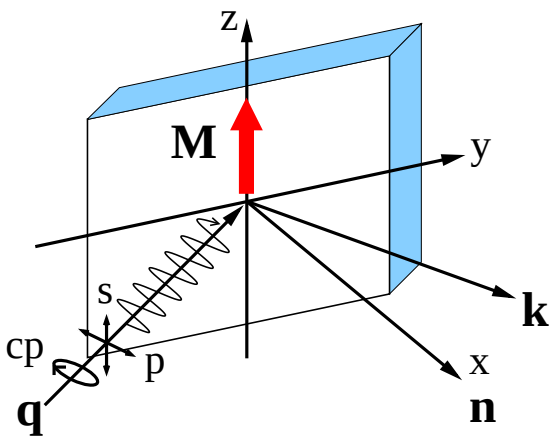

Figure 1. Schematic geometry in the MDAD experiment. The MDAD depends on the relative orientation of the electron emission direction $\boldsymbol{k}$, the direction of photon incidence $\boldsymbol{q}$ and the direction of magnetization $\boldsymbol{M}$. MDAD may be observed for circularly polarized light (cp) as well as for linearly polarized light (s,p).

model for crystalline systems [7, 22, 23]. The outgoing electron is scattered at the other atoms on the way out. The interference of these scattered waves and the primary wave gives rise to intensity modulations and, therefore, to modulations in the magnetic dichroism.

There are experimental results which clearly emphasize the influence of PD effects. Fanelsa *et al* [16] conducted an experiment which directly probed the influence of PD effects. A qualitative explanation of the measured effects was given using a simple two-atom scattering model. This work has been continued and expanded by Schellenberg *et al* [24]. Hillebrecht *et al* [25, 26] measured strong modulations on MLDAD of Fe 3p and Co 3p photoemission in contrast to atomic prediction. Most of the features could be explained within a plane-wave single-scattering PD theory.

By rotating the sample around the direction of magnetization, a strong MLDAD of photoelectrons has been observed in thin Fe and Co layers [27, 28]. This behaviour is in contrast to the single-atom approach, where the MLDAD should be independent of the angle of electron emission if the angle between the electron emission and light incidence is fixed.

In this paper, a PD theory based on the multiple scattering of spherical waves is applied to include PD effects in the theory of MDAD of photoelectrons. The initial state of photoelectrons is considered as a spin–orbit split core state with total angular-momentum quantum number $j_c = l_c \pm 1/2$. Within a one-electron theory of ferromagnetism [21], the only effect of the magnetic solid is to induce an exchange splitting of the different corresponding sublevels $\mu_c = -j_c, -j_c + 1, \ldots, j_c$. Therefore, the intensity of photoelectrons is calculated for each sublevel $|j_c l_c \mu_c\rangle$ within PD theory, which has been applied with success to the discussion of spin polarization and non-magnetic circular dichroism in photoemission [28–32].

In section 2 the basic ingredients of applied PD theory are summarized. For a rough discussion of the influence of PD effects the plane-wave single-scattering approximation is introduced. The results of dipole selection rules are presented in section 3. In tables 1 and 2 the dipole matrix elements are given for $p_{3/2}$ and $p_{1/2}$ core-level photoemission as a function of the polarization of light. The angular dependence of magnetic dichroism and spin polarization is investigated for p-type core-level photoemission in section 4. Numerical results for Co and Fe thin layers are presented in section 5.

2. Multiple-scattering cluster model

The intensity of emitted core-level photoelectrons depends on the emission direction ($\boldsymbol{k} = k\hat{\boldsymbol{k}}$), the photoelectron spin (quantum number σ), the kinetic energy ($E = \hbar^2 k^2/2m$) and the photon polarization vector $\vec{\epsilon}$ [33, 34]

$$I_c^{\sigma}(\boldsymbol{k}, \vec{\epsilon}) \propto \sum_{\boldsymbol{R}_0} \left| \sum_L B_L^{\sigma,\boldsymbol{R}_0}(\boldsymbol{k}) M_{L,c}^{\sigma}(E, \vec{\epsilon}) \right|^2 . \tag{1}$$

The sum about $\boldsymbol{R}_0$ in (1) runs over all contributions of different emitters at site $\boldsymbol{R}_0$, where the photon is absorbed creating a hole state c. The core state c is split by the spin–orbit interaction and its spin and angular part $|c\rangle = |j_c l_c \mu_c\rangle$ is characterized by the angular-momentum quantum number l_c, the total angular-momentum quantum number $j_c = l_c \pm 1/2$ and the related magnetic quantum number $\mu_c = -j_c, -j_c + 1, \ldots, j_c$ [34].

The letter L in the second sum in (1) is an abbreviation for the angular quantum number l and the related magnetic quantum numbers $m = -l, -l + 1, \ldots, l$ of the final state of photoelectrons. Which L-values will contribute to the intensity (1) is determined by the dipole matrix element

$$M_{L,c}^{\sigma}(E, \vec{\epsilon}) = \exp(\mathrm{i}\delta_l) \langle \phi_l | r | \phi_{j_c l_c} \rangle \langle L, \sigma | \hat{\boldsymbol{r}} \cdot \vec{\epsilon} | j_c l_c \mu_c \rangle . \tag{2}$$

From the angular part $\langle L, \sigma | \hat{\boldsymbol{r}} \cdot \vec{\epsilon} | j_c l_c \mu_c \rangle$ in (2) it follows that only the values $l = l_c \pm 1$ are allowed within the dipole approximation. The radial part $R_l = \exp(\mathrm{i}\delta_l) \langle \phi_l | r | \phi_{j_c l_c} \rangle$ in (2) determines the weight of these two contributions, where ϕ_l and $\phi_{j_c l_c}$ are the radial wavefunction of the final and initial state of the photoelectrons, respectively.

The so-called scattering path operator in (1) [33]

$$\begin{aligned} B_L^{\sigma,\boldsymbol{R}_0}(\boldsymbol{k}) = {} & \mathrm{e}^{-\mathrm{i}\boldsymbol{k}\cdot\boldsymbol{R}_0} (-\mathrm{i})^l Y_L(\hat{\boldsymbol{k}}) + \sum_{\boldsymbol{R}' \neq \boldsymbol{R}_0} \sum_{L'} \mathrm{e}^{-\mathrm{i}\boldsymbol{k}\cdot\boldsymbol{R}'} (-\mathrm{i})^{l'} Y_{L'}(\hat{\boldsymbol{k}}) (-\mathrm{i}k t_{l'}^{\sigma}) G_{L'L}(\boldsymbol{R}' - \boldsymbol{R}_0) \\ & + \sum_{\boldsymbol{R}'' \neq \boldsymbol{R}'} \sum_{\boldsymbol{R}' \neq \boldsymbol{R}_0} \sum_{L''} \sum_{L'} \mathrm{e}^{-\mathrm{i}\boldsymbol{k}\cdot\boldsymbol{R}''} (-\mathrm{i})^{l''} Y_{L''}(\hat{\boldsymbol{k}}) \\ & \times (-\mathrm{i}k t_{l''}^{\sigma}) G_{L''L'}(\boldsymbol{R}'' - \boldsymbol{R}') (-\mathrm{i}k t_{l'}^{\sigma}) G_{L'L}(\boldsymbol{R}' - \boldsymbol{R}_0) \\ & + \ldots \end{aligned} \tag{3}$$

contains, besides the direct contribution (first term), the single (second term) and multiple scattering contributions (figure 2). The single site scattering matrix t_l in (3) is defined as $t_l = -k^{-1} \exp(\mathrm{i}\delta_l) \sin\delta_l$, where the scattering phase shifts δ_l for the different kinds of atoms depend on the kinetic energy of photoelectrons and, for magnetic materials, on the spin σ. $G_{L'L}$ is the matrix element of the Green's operator [35] and Y_L represents the spherical harmonic of the first kind [36]. Both the maximum number of partial waves $L', L'', \ldots$ and scattering atoms $\boldsymbol{R}', \boldsymbol{R}'', \ldots$ in (3) depend on the kinetic energy of electrons.

For a rough discussion of the influence of photoelectron diffraction effects the scattering path operator (3) is considered in the plane-wave approximation which means the replacement of $G_{L'L}$ in (3) by its asymptotic value for $kR \gg l'(l' + 1)$ [31, 33] (figure 3). Then the scattering path operator in the single-scattering approach for an emitter in the origin ($\boldsymbol{R}_0 = 0$) and scattering atoms in position $\boldsymbol{R}_j$ can be written in the form

$$B_L(\boldsymbol{k}) \approx (-\mathrm{i})^l Y_L(\hat{\boldsymbol{k}}) + \sum_{j \neq 0} \frac{1}{R_j} f(\theta_{s,j}) \, \mathrm{e}^{\mathrm{i}kR(1-\cos\theta_{s,j})} (-\mathrm{i})^l Y_L(\hat{\boldsymbol{R}}_j) . \tag{4}$$

The quantity $f(\theta_s) = |f(\theta_s)| \mathrm{e}^{\mathrm{i}\psi_s(\theta_s)}$ in (4) is the complex scattering amplitude

$$f(\theta_s) = -\sum_{l=0,1,2\ldots} (2l + 1) t_l P_l(\cos\theta_s) \tag{5}$$

Table 1. Dipole matrix elements $\langle L, \sigma | \boldsymbol{r} \cdot \vec{\epsilon} | j_c l_c \mu_c \rangle \sqrt{4\pi}$ for the excitation of the $p_{3/2}$ core level.

μ_c	$j_c = 3/2, \sigma = 1/2$
3/2	$(-\delta_{L,00} + \sqrt{\frac{1}{5}}\delta_{L,20})c_{-1} + \sqrt{\frac{3}{5}}\delta_{L,21}c_0 + \sqrt{\frac{6}{5}}\delta_{L,22}c_1$
1/2	$\sqrt{\frac{2}{3}}[\sqrt{\frac{3}{5}}\delta_{L,2-1}c_{-1} + (\delta_{L,00} + \sqrt{\frac{4}{5}}\delta_{L,20})c_0 + \sqrt{\frac{3}{5}}\delta_{L,21}c_1]$
−1/2	$\sqrt{\frac{1}{3}}[\sqrt{\frac{6}{5}}\delta_{L,2-2}c_{-1} + \sqrt{\frac{3}{5}}\delta_{L,2-1}c_0 + (-\delta_{L,00} + \sqrt{\frac{1}{5}}\delta_{L,20})c_1]$
−3/2	0
μ_c	$j_c = 3/2, \sigma = -1/2$
3/2	0
1/2	$\sqrt{\frac{1}{3}}[(-\delta_{L,00} + \sqrt{\frac{1}{5}}\delta_{L,20})c_{-1} + \sqrt{\frac{3}{5}}\delta_{L,21}c_0 + \sqrt{\frac{6}{5}}\delta_{L,22}c_1]$
−1/2	$\sqrt{\frac{2}{3}}[\sqrt{\frac{3}{5}}\delta_{L,2-1}c_{-1} + (\delta_{L,00} + \sqrt{\frac{4}{5}}\delta_{L,20})c_0 + \sqrt{\frac{3}{5}}\delta_{L,21}c_1]$
−3/2	$\sqrt{\frac{6}{5}}\delta_{L,2-2}c_{-1} + \sqrt{\frac{3}{5}}\delta_{L,2-1}c_0 + (-\delta_{L,00} + \sqrt{\frac{1}{5}}\delta_{L,20})c_1$

Table 2. Dipole matrix elements as in table 1 for $p_{1/2}$.

μ_c	$j_c = 1/2, \sigma = 1/2$
1/2	$-\sqrt{\frac{1}{3}}[\sqrt{\frac{3}{5}}\delta_{L,2-1}c_{-1} + (\delta_{L,00} + \sqrt{\frac{4}{5}}\delta_{L,20})c_0 + \sqrt{\frac{3}{5}}\delta_{L,21}c_1]$
−1/2	$-\sqrt{\frac{2}{3}}[\sqrt{\frac{6}{5}}\delta_{L,2-2}c_{-1} + \sqrt{\frac{3}{5}}\delta_{L,2-1}c_0 + (-\delta_{L,00} + \sqrt{\frac{1}{5}}\delta_{L,20})c_1]$
μ_c	$j_c = 1/2, \sigma = -1/2$
1/2	$\sqrt{\frac{2}{3}}[(-\delta_{L,00} + \sqrt{\frac{1}{5}}\delta_{L,20})c_{-1} + \sqrt{\frac{3}{5}}\delta_{L,21}c_0 + \sqrt{\frac{6}{5}}\delta_{L,22}c_1]$
−1/2	$\sqrt{\frac{1}{3}}[\sqrt{\frac{3}{5}}\delta_{L,2-1}c_{-1} + (\delta_{L,00} + \sqrt{\frac{4}{5}}\delta_{L,20})c_0 + \sqrt{\frac{3}{5}}\delta_{L,21}c_1]$

well known from quantum mechanics theory [37]. The Legendre polynomial in (5) depends on the scattering angle θ_s between the direction of the observer $\boldsymbol{k}$ and the axis between emitter and scattering atom $\boldsymbol{R}$ (figure 3).

The consideration of the plane-wave approximation comes from the fact that the high-energy photoelectrons emitted from a particular atom are scattered by neighbouring atoms predominantly in the forward-scattering direction ($\theta_s = 0^\circ$). This means that one can expect an enhancement of photoelectron intensity along such directions, which include the emitting atom and one or more neighbours.

The ineleastic mean free path, the Debye–Waller factor and refraction at the surface barrier can be included in the usual way [35, 38]. In the case of non-magnetic material the sublevels μ_c are degenerated and, therefore, the intensity of photoelectrons is determined by the incoherent sum over all μ_c in (1).

3. Dipole selection rules

For the calculation of the dipole matrix element (2) the product $\hat{\boldsymbol{r}} \cdot \vec{\epsilon}$ is written as

$$\hat{\boldsymbol{r}} \cdot \vec{\epsilon} = \sum_{m=-1}^{1} c_m \, Y_{1m}(\hat{\boldsymbol{r}}). \tag{6}$$

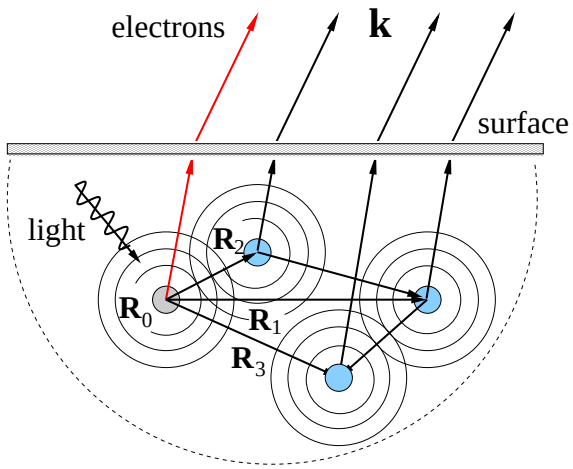

Figure 2. Multiple-scattering cluster model. The interference of the direct wave (emitted at $\boldsymbol{R}_0$) and the scattered waves (atoms at $\boldsymbol{R}_1$, $\boldsymbol{R}_2$, $\boldsymbol{R}_3$, dots) causes modulations in the angular dependence of the photoelectron intensity.

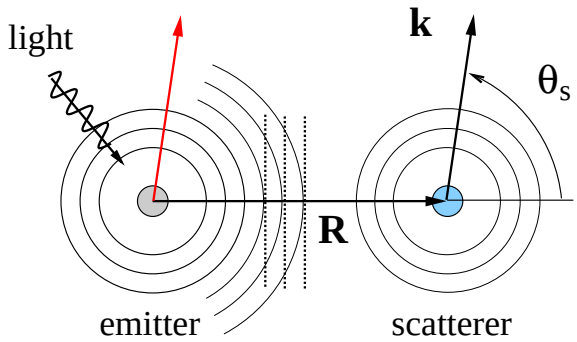

Figure 3. Plane-wave approximation. The emitted spherical wave is approximated by a plane wave.

The quantities c_m are determined by

$$c_{-1} = \sqrt{\frac{2\pi}{3}}(\epsilon_x + \mathrm{i}\epsilon_y) \qquad c_0 = \sqrt{\frac{4\pi}{3}}\epsilon_z \qquad c_1 = -\sqrt{\frac{2\pi}{3}}(\epsilon_x - \mathrm{i}\epsilon_y) \tag{7}$$

where $(\epsilon_x, \epsilon_y, \epsilon_z)$ are the components of the polarization vector $\vec{\epsilon}$. The spin–orbit state $|j_c l_c \mu_c\rangle$ can be constructed from the Clebsch–Gordan coefficients and the eigenstates $|L_c, \sigma_c\rangle$ [37]. The spin and angular part of the dipole matrix element is then given by

$$\langle L, \sigma | \hat{\boldsymbol{r}} \cdot \vec{\epsilon} | j_c l_c \mu_c \rangle = \begin{cases} \pm\sqrt{\dfrac{l_c \pm \mu_c + \frac{1}{2}}{2l_c + 1}} \displaystyle\sum_{m'=-1}^{1} c_{m'} \int \mathrm{d}\Omega\, Y_L^*(\hat{\boldsymbol{r}}) Y_{1m'}(\hat{\boldsymbol{r}}) Y_{l_c, \mu_c - \frac{1}{2}}(\hat{\boldsymbol{r}}) \\ \qquad \text{for } \sigma = +\frac{1}{2} \text{(spin up)} \\ \sqrt{\dfrac{l_c \mp \mu_c + \frac{1}{2}}{2l_c + 1}} \displaystyle\sum_{m'=-1}^{1} c_{m'} \int \mathrm{d}\Omega\, Y_L^*(\hat{\boldsymbol{r}}) Y_{1m'}(\hat{\boldsymbol{r}}) Y_{l_c, \mu_c + \frac{1}{2}}(\hat{\boldsymbol{r}}) \\ \qquad \text{for } \sigma = -\frac{1}{2} \text{(spin down).} \end{cases} \tag{8}$$

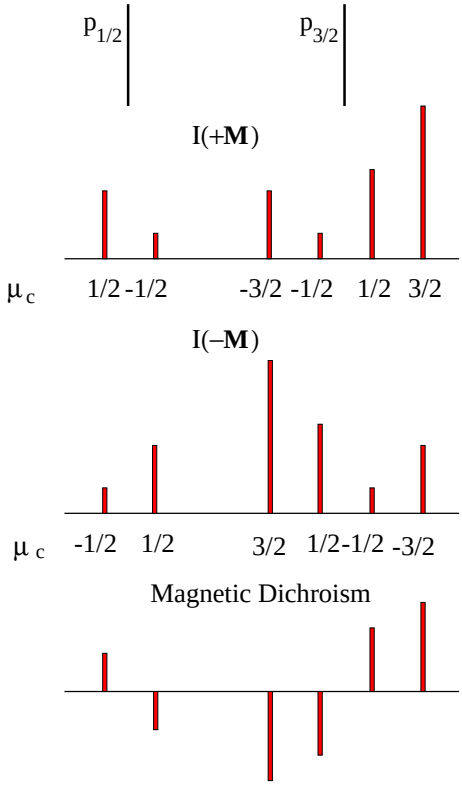

Figure 4. One-electron theory of magnetic dichroism. The actually degenerated μ_c sublevels of the spin–orbit split core states $p_{3/2}$ and $p_{1/2}$ are separated energetically by an exchange interaction. Reversing the magnetization merely interchanges the energetic position of $|j_c l_c \mu_c\rangle$ and $|j_c l_c, -\mu_c\rangle$.

The selection rules of the contributing partial waves L in the final state are given for the excitation of $p_{1/2}$ and $p_{3/2}$ core-level photoemission in tables 1 and 2, respectively.

4. Magnetic dichroism and spin polarization

Within a one-electron model of ferromagnetism [21] the actual degenerated μ_c sublevels of both the spin–orbit split core states $j_c = l_c \pm 1/2$ are separated energetically by an exchange interaction. Reversing the magnetization merely interchanges the energetic position of $|j_c l_c \mu_c\rangle$ and $|j_c l_c, -\mu_c\rangle$ as shown in figure 4. Therefore, the magnetic dichroism may be calculated simply by considering a single magnetic orientation and taking the intensity difference $I_{j_c,\mu_c} - I_{j_c,-\mu_c}$. In dependence on the experimental conditions the magnetic dichroism is determined by a sum of all contributing differences $I_{j_c,\mu_c} - I_{j_c,-\mu_c}$ of the considered core level.

This model of ferromagnetism is applied to the calculation of the MDAD of p-type core-level photoemission. For the $p_{3/2}$ core level the intensity difference of $\mu_c = \pm 3/2$ is given by

$$I_{\frac{3}{2},\frac{3}{2}} - I_{\frac{3}{2},-\frac{3}{2}} = \sum_{\sigma} I^{\sigma}_{\frac{3}{2},\frac{3}{2}} - \sum_{\sigma} I^{\sigma}_{\frac{3}{2},-\frac{3}{2}} = I^{\uparrow}_{\frac{3}{2},\frac{3}{2}} - I^{\downarrow}_{\frac{3}{2},-\frac{3}{2}}. \tag{9}$$

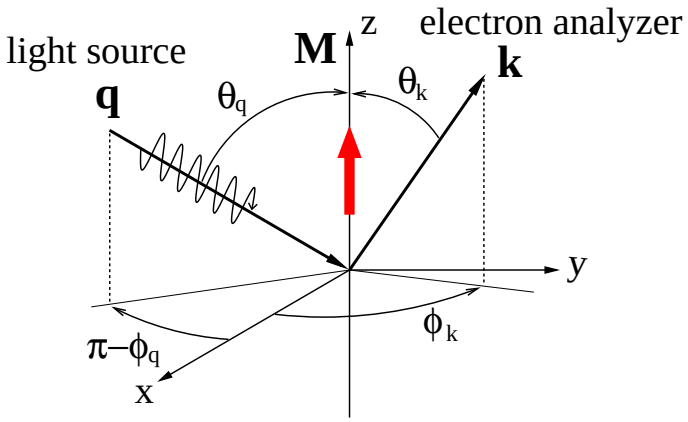

Figure 5. Schematic geometry. The magnetization and spin quantization axes are along the $+z$-axis.

The intensity differences of $\mu_c = \pm 1/2$ for $p_{3/2}$

$$I_{\frac{3}{2},\frac{1}{2}} - I_{\frac{3}{2},-\frac{1}{2}} = I^{\downarrow}_{\frac{3}{2},\frac{1}{2}} - I^{\uparrow}_{\frac{3}{2},-\frac{1}{2}} = \tfrac{1}{3}[I^{\uparrow}_{\frac{3}{2},\frac{3}{2}} - I^{\downarrow}_{\frac{3}{2},-\frac{3}{2}}] \tag{10}$$

and $p_{1/2}$

$$I_{\frac{1}{2},\frac{1}{2}} - I_{\frac{1}{2},-\frac{1}{2}} = I^{\downarrow}_{\frac{1}{2},\frac{1}{2}} - I^{\uparrow}_{\frac{1}{2},-\frac{1}{2}} = \tfrac{2}{3}[I^{\uparrow}_{\frac{3}{2},\frac{3}{2}} - I^{\downarrow}_{\frac{3}{2},-\frac{3}{2}}], \tag{11}$$

respectively, differ only by a factor $\frac{1}{3}$ and $\frac{2}{3}$ from (9), respectively.

The spin polarization in core-level photoemission is defined as the difference between the total intensity of spin-up and spin-down electrons

$$I^{\uparrow}_{j_c} - I^{\downarrow}_{j_c} = \sum_{\mu_c} I^{\uparrow}_{j_c,\mu_c} - \sum_{\mu_c} I^{\downarrow}_{j_c,\mu_c}. \tag{12}$$

According to the relations provided in tables 1 and 2, the spin polarization of the $p_{3/2}$ core level is given by

$$I^{\uparrow}_{3/2} - I^{\downarrow}_{3/2} = \tfrac{2}{3}[I_{\frac{3}{2},\frac{3}{2}} - I_{\frac{3}{2},-\frac{3}{2}}] \tag{13}$$

and of the $p_{1/2}$ core level by

$$I^{\uparrow}_{1/2} - I^{\downarrow}_{1/2} = -[I^{\uparrow}_{3/2} - I^{\downarrow}_{3/2}], \tag{14}$$

respectively.

Therefore, spin polarization and dichroism should show the same dependence on the emission direction of photoelectrons provided that the energy difference due to the spin–orbit interaction between the $p_{1/2}$ and $p_{3/2}$ core levels and the influence of magnetic scattering are small.

5. MDAD of p-type core-level photoemission

The MDAD depends on the relative directions of light incidence $\boldsymbol{q}$, electron emission $\boldsymbol{k}$ and magnetization $\boldsymbol{M}$, as well as on polarization properties of light. In the following discussion both the direction of magnetization $\boldsymbol{M}$ and the spin quantization axis are considered to be directed along the $+z$-axis. The direction of light incidence $\boldsymbol{q}$ and electron emission $\boldsymbol{k}$ are given by the related polar and azimuthal angles (θ, ϕ), respectively (figure 5).

First, linearly polarized light is considered incident in the xy-plane ($\theta_q = 90^\circ$) with arbitrary azimuthal angle ϕ_q. According to the selection dipole rules (tables 1 and 2) for p-polarized light with polarization vector $\vec{\epsilon} = (-\sin\phi_q, \cos\phi_q, 0)$ the intensity difference (9) is determined by

$$I_{\frac{3}{2},\frac{3}{2}} - I_{\frac{3}{2},-\frac{3}{2}} \propto \sqrt{\tfrac{6}{5}}(|B_{22}|^2 - |B_{2-2}|^2)|R_2|^2 \qquad (15)$$
$$+2\mathrm{Re}\,[(-B_{00}R_0 + \sqrt{\tfrac{1}{5}}B_{20}R_2)(B_{22}^*\,\mathrm{e}^{\mathrm{i}2\phi_q} - B_{2-2}^*\,\mathrm{e}^{-\mathrm{i}2\phi_q})R_2^*]$$

where $R_2 = |R_2|\exp(\mathrm{i}\delta_2)$ and $R_0 = |R_0|\exp(\mathrm{i}\delta_0)$ in (15) are the radial matrix elements for the d ($l = 2$) and s ($l = 0$) channel, respectively.

For s-polarized light with polarization vector $\vec{\epsilon} = \boldsymbol{e}_z$ along the z-axis the intensity difference

$$I_{\frac{3}{2},\frac{3}{2}} - I_{\frac{3}{2},-\frac{3}{2}} \propto |B_{21}|^2 - |B_{2-1}|^2 \qquad (16)$$

does not vanish in general. If the electron is detected within the plane perpendicular to $\boldsymbol{M}$ the direct contribution to the scattering path operator $B_{2\pm1}$ vanishes and without the interference between the direct and scattered contribution the difference (16) will vanish too.

For a first insight into the angular dependence of the magnetic dichroism only a single atom in the origin of the coordinate system is considered. Within this single-atom approach just the first term of B_L in (3), $(-\mathrm{i})^l Y_L(\theta_k, \phi_k)$, has to be taken into account, where θ_k and ϕ_k are the polar and azimuthal angles of $\hat{\boldsymbol{k}}$, respectively. To distinguish the single-atom approach from the general case of photoelectron diffraction the intensity difference (9) is called $MD^{(0)}$ in the following paragraphs. Within the single-atom approach the intensity difference of s-polarized light (16) vanishes and the difference of p-polarized light (15) is simplified to

$$MD^{(0)} \propto |R_0|\,|R_2|\sin(\delta_0 - \delta_2)\sin^2\theta_k \sin 2(\phi_k - \phi_q) \qquad (17)$$

respectively. This angular dependence is well known from other atomic approaches of magnetic dichroism in photoemission, especially for normal incidence of light where $\phi_q = 0^\circ$.

Only taking into account the interference between s- and d-waves for the excitation of the p-level, the magnetic dichroism (17) does not vanish from the start. The sign of the difference (17) depends on the sign of the difference of the phase shifts $(\delta_0 - \delta_2)$. In the case of circularly polarized light the intensity difference (9) for the MDAD is considered in dependence on the incident direction of light. If $\boldsymbol{q}$ is parallel to the z-axis and therefore parallel to $\boldsymbol{M}$, the polarization vector $\vec{\epsilon} = (\boldsymbol{e}_x \pm \mathrm{i}\boldsymbol{e}_y)/\sqrt{2}$ gives light of positive or negative helicity, respectively. For the intensity difference (9) yields

$$I_{\frac{3}{2},\frac{3}{2}} - I_{\frac{3}{2},-\frac{3}{2}} \propto (\tfrac{6}{5}|B_{2\pm2}|^2 - \tfrac{1}{5}|B_{20}|^2)|R_2|^2 + |B_{00}|^2|R_0|^2 + 2\mathrm{Re}\,(B_{00}R_0\tfrac{1}{\sqrt{5}}B_{20}^*R_2^*) \qquad (18)$$

which is simplified within the single-atom approach to

$$MD^{(0)} \propto |R_2|^2(3\sin^2\theta_k - 1) - |R_0|(|R_0| + |R_2|(3\cos^2\theta_k - 1)\cos(\delta_0 - \delta_2)). \qquad (19)$$

In this case dichroism may be observed for pure s- or d-waves. The dichroism does not depend on ϕ_k and does not vanish for $\theta_k = 0^\circ$ or $\theta_k = 90^\circ$.

For completeness, the magnetic dichroism for circularly polarized light incident normal to $\boldsymbol{M}$ with polarization vector $\vec{\epsilon} = (\boldsymbol{e}_y \pm \mathrm{i}\boldsymbol{e}_z)/\sqrt{2}$ is written within the single-atom approach

$$MD^{(0)} \propto \mp|R_2|\sin\theta_k\cos\phi_k[|R_2|\cos\theta_k + |R_0|(\cos\theta_k\cos(\delta_0 - \delta_2)$$
$$\mp \sin\theta_k\sin\phi_k\sin(\delta_0 - \delta_2))] \qquad (20)$$

which gives for electron detection in the xy-plane ($\theta_k = 90^\circ$) again the well known angular dependence $MD^{(0)} \propto \mp|R_0||R_2|\sin(\delta_0 - \delta_2)\sin 2\phi_k$.

For the discussion of the influence of PD effects on the MDAD the scattering path operator B_L is considered in the plane-wave approximation (4). As the simplest model, only a single scattering atom in position $\boldsymbol{R} = R\boldsymbol{e}_y$ is assumed. Again, linearly polarized light with $\vec{\epsilon} = \boldsymbol{e}_y$ is considered. The angular dependence of the magnetic dichroism $MD^{(0)}$ (17) is now modulated due to the scattering of the emitted electron wave on the atom in position $\boldsymbol{R}$

$$MD^{(1)} \propto [|R_0|\,|R_2|(\sin(\delta_0 - \delta_2) + F\sin(\delta_0 - \delta_2 - \psi)) - 2F\sin\psi|R_2|^2]\sin^2\theta_k \sin 2\phi_k \tag{21}$$

where $F = |f(\theta_s)|/R$ and $\psi = kR(1 - \cos\theta_s) + \psi_s(\theta_s)$ in (21) are related to the amount and the phase of the complex scattering amplitude $f(\theta_s)$ (5), respectively. The scattering angle θ_s is determined by $\cos\theta_s = \sin\phi_k \sin\theta_k$. In the limit $F = 0$ (no scattering) the angular dependence of the single-atom approach (17) follows.

Even this simple model demonstrates the influence of PD effects on the magnetic dichroism in plain terms. The angular dependence of the magnetic dichroism may be modulated strongly by PD effects and may thus differ from the atomic behaviour. The last statement is particularly important for experimental geometries where the angle between light incidence and electron emission is fixed and the sample is rotated around a fixed axis. It may be helpful to consider again the result of the simple two-atom cluster. Due to rotation around the z-axis the position of the scattering atom is changed which is determined by the azimuthal angle ϕ_R of the atom. For electron detection along the x-axis (corresponding to normal emission) and light incidence in the xy-plane with $\phi_q = 45^\circ$, the intensity difference is determined by

$$\begin{aligned} MD^{(1)} \propto {} & F\sin\psi|R_2|^2(1 - \cos 2\phi_R - 3\sin 2\phi_R) - 2|R_0||R_2|[\sin(\delta_0 - \delta_2)(1 + F^2\cos 2\phi_R) \\ & +2F(\cos 2\phi_R \sin(\delta_0 - \delta_2 - \psi) + \sin(\delta_0 - \delta_2 + \psi))] \end{aligned} \tag{22}$$

where F and ψ in (22) depend on the angle ϕ_R of the scatterer.

The examples considered emphasize the importance of PD effects in the angular dependence of magnetic dichroism. Both simple arrangements of atoms and the plane-wave approximation may help to estimate this contribution. For the explanation of experimental data the full PD theory according to (3) is applied.

6. Numerical results for Fe and Co

The PD theory has been applied to calculate the MLDAD of thin Fe layers. The position of the light source is fixed normal to the surface and the electron analyser is rotated within the plane of incidence (figure 6). The magnetization is considered to be in the surface plane along [010]. The angle of electron emission with respect to the surface normal is called the polar angle θ. In figure 7 the calculated intensity (1) and the related magnetic dichroism (9) are shown for Fe 3p core-level photoemission in Fe(001) excited by linearly p-polarized light. The dependence of the intensity and the magnetic dichroism on the polar angle has been calculated for two different azimuthal direction of a small Fe(001) cluster within the single-scattering approach. The thin smooth lines in figure 7 represent the result derived for the single-atom model, where the difference (lower part) follows $\sin 2\theta$. The calculation emphasizes the importance of PD effects in the considered electron energy region about 100 eV where a strong modulation of the single-atom result is observed. The calculated data are in good agreement with the experimental results of Hillebrecht *et al* [25].

As a second example the intensity and related magnetic dichroism have been considered for Co 2p photoelectrons excited by unpolarized Mg Kα radiation ($h\nu = 1253.6$ eV) in five Co monolayers (ML) on a Cu(001) substrate. Both theoretical results (full curve) and experimental results (full squares) are shown in figure 8. In the experiment the MDAD has been measured

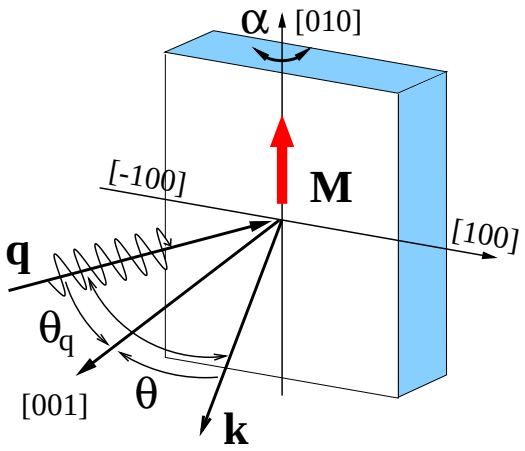

Figure 6. Experimental geometry of measuring MDAD.

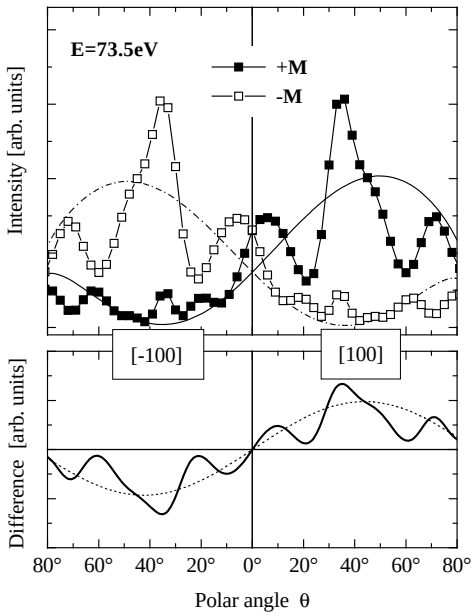

Figure 7. Angular dependence of the intensity of Fe 3p photoelectron in Fe(001) excited by linearly polarized light and the related magnetic dichroism. Due to PD effects the single-atom approach $\sin 2\theta$ is strongly modulated.

by reversing the magnetization which is in the surface plane parallel to the [010] direction [28]. The sample has been rotated around the axis of magnetization (rotation angle α) whereby the angle between the electron emission $\boldsymbol{k}$ and the photon incidence $\boldsymbol{q}$ remains at 45° (figure 6). The angle $\alpha = 0^\circ$ corresponds to normal electron emission.

The theoretical data in figure 8 have been calculated within a single-scattering approach for a cluster of five ML of Co atoms on the assumption that the Co atoms continue the Cu(001) bulk structure. The influence of diffraction effects due to the Cu substrate can be neglected because of the strong forward scattering of the Co 2p photoelectrons in the energy region considered. The unpolarized light has been considered as a superposition of linearly

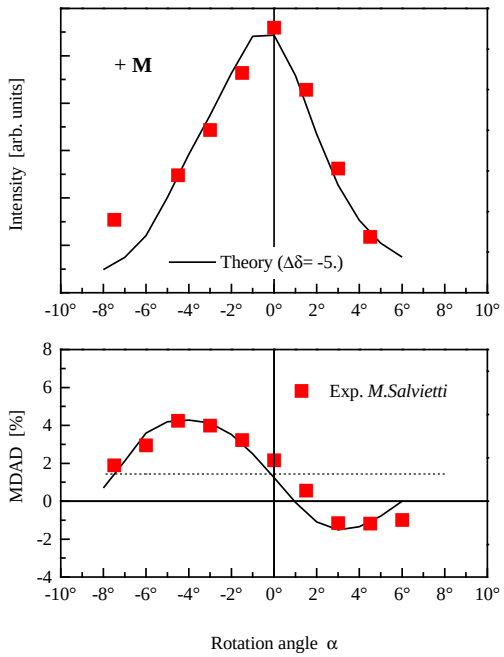

Figure 8. Magnetic dichroism in the angular distribution of Co 2p photoelectrons in five ML Co/Cu(001). The sample is rotated around the direction of magnetization (figure 6) [28].

p-polarized and s-polarized light, whereby the s-polarized part does not contribute to the magnetic dichroism.

Obviously, there is a good agreement between experiment and theory for both intensity (upper part in figure 8) and magnetic dichroism (lower part in figure 8). The dashed line in the lower part of figure 8 gives the result of the magnetic dichroism in the single-atom approach which is constant. Therefore, the angular dependence is caused by PD effects. The sign of the magnetic dichroism for normal emission of electrons depends on the sign of the difference $\Delta = \delta_0 - \delta_2$. This difference has been fitted and the best agreement has been obtained with $\Delta = -5$ in the calculation.

7. Conclusions

PD theory in conjunction with a one-electron theory of ferromagnetism gives the possibility of a better understanding of the influence of PD effects on the angular dependence of magnetic dichroism. The applied theory of a multiple-scattering cluster model offers a simple insight and an estimation of the influence of PD effects. As shown for the excitation of p-type photoelectrons in thin Co and Fe layers, the observed modulations in the MDAD are explained very well. The application of this theory depends on the validity of the one-electron model of ferromagnetism. This approach clearly breaks down for a localized atomic-like system, where coupling between the core hole and the valence shell results in a complex multiplet structure.

Furthermore, the study of MDAD allows the determination of the phase difference $(\delta_0 - \delta_2)$, as shown for Co 2p, if the experiment is carried out in the proper geometry.

References

[1] Baumgarten L, Schneider C M, Petersen H, Schäfer F and Kirschner J 1990 *Phys. Rev. Lett.* **65** 492
[2] Ebert H, Baumgarten L, Schneider C M and Kirschner J 1991 *Phys. Rev.* B **44** 4406
[3] van der Laan G 1991 *Phys. Rev. Lett.* **66** 2527
van der Laan G 1991 *J. Phys.: Condens. Matter* **3** 1015
Thole B T and van der Laan G 1991 *Phys. Rev. Lett.* **67** 3306
[4] Schneider C M, Venus D and Kirschner J 1992 *Phys. Rev.* B **45** 5041
[5] Venus D, Baumgarten L, Schneider C M, Boeglin C and Kirschner J 1993 *J. Phys.: Condens. Matter* **5** 1239
[6] Waddill G D, Tobin J G and Pappas D P 1992 *Phys. Rev.* B **46** 552
Pappas D P, Waddill G D and Tobin J G 1993 *J. Appl. Phys.* **73** 5936
[7] Tamura E, Wadill G D, Tobin J G and Sterne P A 1994 *Phys. Rev. Lett.* **73** 1533
[8] Starke K, Navas E, Baumgarten L and Kaindl G 1993 *Phys. Rev.* B **48** 1329
[9] Arenholz E, Navas E, Starke K, Baumgarten L and Kaindl G 1995 *Phys. Rev.* B **51** 8211
Arenholz E, Starke K and Kaindl G 1995 *J. Electron. Spectroc. Relat. Phenom.* **76** 183
Arenholz E, Starke K, Navas E and Kaindl G 1996 *J. Electron. Spectrosc.* **78** 241
[10] van der Laan G, Arenholz E, Navas E, Bauer A and Kaindl G 1996 *Phys. Rev.* B **53** R5998
[11] Roth Ch, Hillebrecht F U, Rose H B and Kisker E 1993 *Phys. Rev. Lett.* **70** 3479
Roth Ch, Rose H B, Hillebrecht F U and Kisker E 1993 *Solid State Commun.* **86** 647
[12] Sirotti F and Rossi G 1994 *Phys. Rev.* B **49** 15 682
Rossi G, Sirotti F, Cherepkov N A, Farnoux F C and Panaccione G 1994 *Solid State Commun.* **90** 557
[13] Kuch W, Lin M T, Steinhögl W, Schneider C M, Venus D and Kirschner J 1995 *Phys. Rev.* B **51** 609
[14] Hillebrecht F U and Herberg W D 1994 *Z. Phys.* B **93** 299
Fanelsa A, Schellenberg R, Hillebrecht F U and Kisker E 1995 *Solid State Commun.* **96** 291
[15] Rossi G, Panaccione G and Sirotti F 1997 *Phys. Rev.* B **55** 11 488
[16] Fanelsa A, Schellenberg R, Hillebrecht F U, Kisker E, Menchero J G, Kaduwela A P, Fadley C S and Van Hove M A 1996 *Phys. Rev.* B **54** 17 962
[17] Getzlaff M, Ostertag Ch, Fecher G H, Cherepkov N A and Schönhense G 1994 *Phys. Rev. Lett.* **73** 3030
[18] Schneider C M, Pracht U, Kuch W, Chassé A and Kirschner J 1996 *Phys. Rev.* B **54** R15 618
[19] Cherepkov N A, Kuznetsov V V and Verbitskii V A 1995 *J. Phys. B: At. Mol. Opt. Phys.* **28** 1221 and references therein
[20] Cherepkov N A 1994 *Phys. Rev.* B **50** 13 813
Cherepkov N A 1994 *J. Phys.: Condens. Matter* **8** 4971
[21] Menchero J G 1998 *Phys. Rev.* B **57** 993
[22] Ebert H and Guo G-Y 1995 *J. Magn. Magn. Mater.* **148** 174
[23] Henk J, Scheunemann T, Halilov S V and Feder R 1996 *J. Phys.: Condens. Matter* **8** 47
[24] Schellenberg R, Kisker E, Fanelsa A, Hillebrecht F U, Menchero J G, Kaduwela A P, Fadley C S and Van Hove M A 1998 *Phys. Rev.* B **57** 14 310
[25] Hillebrecht F U, Rose H B, Kinishita T, Idzerda Y U, van der Laan G, Denecke R and Ley L 1995 *Phys. Rev. Lett.* **75** 2883
[26] Hillebrecht F U, Rose H B, Roth Ch and Kisker E 1995 *J. Magn. Magn. Mater.* **148** 49
Rose H B, Hillebrecht F U, Kisker E, Denecke R and Ley L 1995 *J. Magn. Magn. Mater.* **148** 62
[27] Gao X, Salvietti M, Kuch W, Schneider C M and Kirschner J 1998 *Phys. Rev.* B **58** 15 426
[28] Salvietti M, Gao X, Kuch W and Kirschner J, to be published
[29] Rennert P, Mück W and Chassé A 1996 *Phys. Rev.* B **53** 14 262
Rennert P, Mück W and Chassé A 1996 *Surf. Sci.* **357–358** 260
[30] Chassé A and Rennert P 1997 *J. Physique IV* **7** C2 427
Rennert P, Chassé A, Nakatani T, Nakatsuji K, Daimon H and Suga S 1997 *J. Phys. Soc. Japan* **66** 396
[31] Chassé A and Rennert P 1997 *Phys. Rev.* B **55** 4120
Chassé A and Rennert P 1997 *J. Electron. Spectrosc. Relat. Phenom.* **87** 91
[32] Chassé A and Rennert P 1997 *J. Phys. Chem. Solids* **58** 509
[33] Rennert P and Chassé A 1987 *Exp. Technik Phys.* **35** 27
Chassé A and Rennert P 1986 *Phys. Status Solidi* b **138** 53
Chassé A 1992 *Surf. Sci.* **269–270** 22
[34] Speder O, Rennert P and Chassé A 1995 *Surf. Sci.* **331–333** 1383
[35] Pendry J B 1974 *Low-Energy Electron Diffraction* (London: Academic)
[36] Abramowitz M and Stegun I A (eds) 1964 *Handbook of Mathematical Functions* (New York: Dover)
[37] Messiah A 1961 *Quantum Mechanics* vol I and II (Amsterdam: North-Holland)
[38] Fadley C S 1993 *Surf. Sci. Rep.* **19** 231
Fadley C S 1993 *Synchrotron Radation Research: Advances in Surface Science* ed R Z Bachrach (New York: Plenum)